Author/s:
Janetzki, JT;Zahir, FZM;Gable, RW;Phonsri, W;Murray, KS;Goerigk, L;Boskovic, C

Title:
A Convenient DFT-Based Strategy for Predicting Transition Temperatures of Valence Tautomeric Molecular Switches

Date:
2021-09-20

Citation:
Janetzki, J. T., Zahir, F. Z. M., Gable, R. W., Phonsri, W., Murray, K. S., Goerigk, L. & Boskovic, C. (2021). A Convenient DFT-Based Strategy for Predicting Transition Temperatures of Valence Tautomeric Molecular Switches. Inorganic Chemistry, 60 (18), pp.14475-14487. https://doi.org/10.1021/acs.inorgchem.1c02273.

Persistent Link:
https://hdl.handle.net/11343/333722

A Convenient DFT-Based Strategy for Predicting Transition Temperatures of Valence Tautomeric Molecular Switches

Jett T. Janetzki,[†,‡] F. Zahra M. Zahir,[†,‡] Robert W. Gable,[†] Wasinee Phonsri,[§] Keith S. Murray,[§] Lars Goerigk,[†] and Colette Boskovic*,[†]*

[†] School of Chemistry, University of Melbourne, Victoria 3010, Australia

[§] School of Chemistry, Monash University, Clayton, Victoria 3800, Australia

ABSTRACT

The ability to identify promising candidate switchable molecules computationally, prior to synthesis, represents a considerable advance in the development of switchable molecular materials. Even more useful would be the possibility of predicting the switching temperature. Cobalt-dioxolene complexes can exhibit thermally-induced valence tautomeric switching between low-spin Co^{III}-catecholate and high-spin Co^{II}-semiquinonate forms, where the half-temperature ($T_{1/2}$) is the temperature at which there are equal amounts of the two tautomers. We report the first simple computational strategy for accurately predicting $T_{1/2}$ values for valence tautomeric (VT) complexes. Dispersion-corrected density functional theory (DFT) methods have been applied to the [Co(dbdiox)(dbsq)(N_2L)] (dbdiox/ dbsq$^{\bullet-}$ = 3,5-di-*tert*-butyldioxolene/semiquinonate; N_2L = diimine) family of VT complexes, including the newly reported [Co(dbdiox)(dbsq)(MeO-bpy)] (**1**) (MeO-bpy = 4,4′-dimethoxy-2,2′-bipyridine). The DFT strategy has been thoroughly benchmarked to experimental data, affording highly accurate spin-distributions and an excellent energy match between experimental and calculated spin-states. Detailed orbital analysis of the [Co(dbdiox)(dbsq)(N_2L)] complexes has revealed that the diimine ligand tunes the $T_{1/2}$ value primarily through π-acceptance. We have established an excellent correlation between experimental $T_{1/2}$ (toluene) values for [Co(dbdiox)(dbsq)(N_2L)] complexes and the calculated lowest unoccupied molecular orbital energy of the corresponding diimine ligand. The model affords accurate $T_{1/2}$ (toluene) values for [Co(dbdiox)(dbsq)(N_2L)] complexes, with an average error of only 3.7%. This quantitative and simple DFT strategy allows experimentalists to not only rapidly identify proposed VT complexes, but also predict the transition temperature. This study lays the groundwork for future *in silico* screening of candidate switchable molecules prior to experimental investigation, with associated time, cost, and environmental benefits.

INTRODUCTION

A molecular approach to the development of switchable spin-bearing materials offers excellent potential for tunability of properties compared to conventional solid-state materials.[1] Molecules that can be interconverted between two or more distinct electronic states upon application of an external stimulus are therefore important synthetic targets.[2–8] Switchable molecules are relevant for future applications in quantum information processing,[3,5] spintronics,[4,9] and thin-films for sensing and displays.[6,7,10,11]

Metal complexes that interconvert between low-spin (LS) and high-spin (HS) state in response to a stimulus, for example upon heating and cooling, have provided numerous examples of switchable spin crossover (SCO) systems.[7,12] Another class of switchable molecules that offers diverse possibilities for applications are those that exhibit valence tautomerism (VT), involving stimulated intramolecular electron transfer between a redox-active metal and coordinated ligand.[13–15] Valence tautomeric interconversions can be triggered by stimuli such as temperature, light, magnetic fields or pressure and VT has been reported for complexes of various metals, including transition, main group and lanthanoid-metals. The range of metal-ligand combinations and the intrinsic redox-activity suggests avenues for multifunctional materials that are not available with SCO compounds. For example, the difference in charge distributions between valence tautomers confers possibilities involving polarization switching and spin-dependent conductivity and electrical properties.[16–20]

Cobalt complexes incoporating dioxolene (diox) ligands in the catecholate (cat^{2-}) or semiquinonate ($sq^{\bullet-}$) oxidation states provide the most numerous examples of VT.[13–15] The first family of such complexes to be studied were the [Co(dbdiox)(dbsq)(N_2L)] (dbdiox/$dbsq^{\bullet-}$ = 3,5-

di-*tert*-butyldioxolene/semiquinonate; N_2L = diimine; Chart 1) series, with thermal VT reported for the 2,2'-bipyridyl (bpy) analogue by Buchanan and Pierpont in 1980.[21] Valence tautomerism in these complexes involves a concerted spin transition and thus interconversion between the low spin (LS) [Co(dbcat)(dbsq)(N_2L)] tautomer at low temperature and the high spin (HS) [Co(dbsq)$_2$(N_2L)] tautomer at high temperature. The transition temperature ($T_{1/2}$) is the temperature at which the two tautomeric forms co-exist in equal amounts. Investigations of several members of the [Co(dbdiox)(dbsq)(N_2L)] family suggested that $T_{1/2}$ values increase with increasing electron-donor ability of the diimine ancillary ligand.[22–24]

Chart 1. Representative LS-Co^{III}-(cat)(SQ) tautomer of [Co(dbdiox)(dbsq)(N_2L)] complexes with the N_2L ligands used in this work.

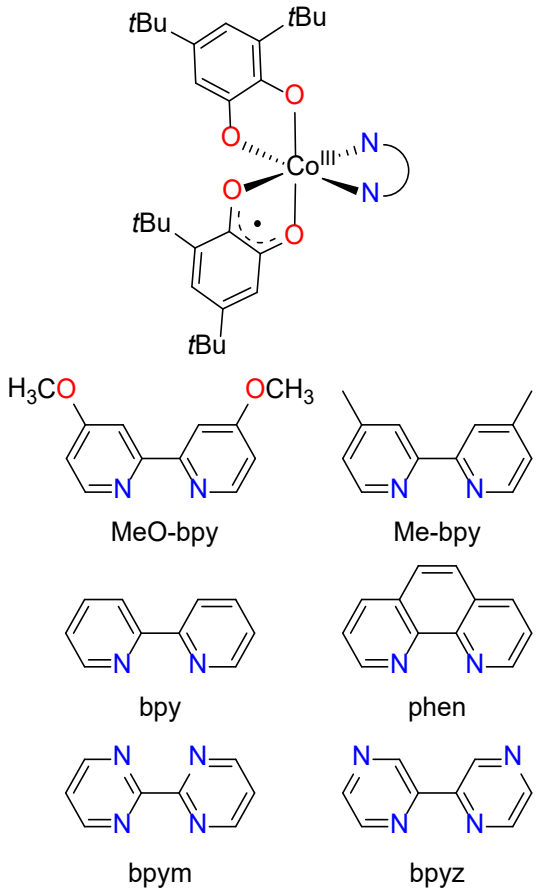

Density functional theory (DFT)[25,26] has become an invaluable tool for chemists to study the structure and properties of molecules. Since the first application of DFT to the [Co(dbdiox)(dbsq)(N_2L)] family of VT complexes in 1997,[27] DFT approaches have been employed on a number of occasions to rationalize experimental observations.[5,15,28–35] However, VT systems are challenging to model using DFT methods: they are open shell species, highly functional dependent, and involve a change in spin state.[36–39] As a result, accurate DFT analysis of VT is non-trivial. Recently, DFT methods have also been employed to predict candidate VT

compounds, which were subsequently verified to exhibit VT experimentally, including by some of us.[39–41] In other cases, DFT predictions are yet to be confirmed via experiments. In contrast, DFT applications on Fe(II) complexes has seen greater development, with several reported efforts to computationally determine whether SCO will occur.[42–48] In a landmark study, Brooker *et al*. developed a simple method to determine transition temperatures of Fe(II) SCO complexes with azine-substituted 1,2,4-triazole ligands, based on a correlation of the solution $T_{1/2}$ values with observed and DFT calculated ^{15}N NMR chemical shift values for ligand resonances.[49]

It is desirable from both environmental and cost standpoints that computational chemistry becomes an essential tool for screening candidate compounds for a targeted property prior to synthesis and experimental investigation. However, the development of efficient and reliable computational methods, together with rigorous benchmarking against experimental data, are both required before computational screening can become routine. The ability to identify systems that will exhibit switching is an important goal, but the next step of accurate prediction of transition temperatures is even more important for developing molecular materials for applications.

Herein we report our efforts to develop computational screening strategies for switchable molecules. We have developed the first efficient DFT strategy for reliable screening of candidate VT molecules and prediction of $T_{1/2}$ values. The [Co(dbdiox)(dbsq)(N_2L)] family of VT complexes was selected for this study as it offers the largest reported range of solution (toluene) $T_{1/2}$ values, as well as forming the basis for various multifunctional materials.[5,19,50–57] Solution $T_{1/2}$ values are crucial as VT in the solid-state is also governed by crystal-packing and supramolecular interactions.[23,58,59] A new member of the family, [Co(dbdiox)(dbsq)(MeO-bpy)] (**1**; MeO-bpy = 4,4′-dimethoxy-2,2′-bipyridine) was first synthesized and characterized to increase the available range of experimental $T_{1/2}$ values for comparison with calculated values. We then developed a

dispersion-corrected DFT protocol incorporating real physical and environmental effects and applied it to the [Co(dbdiox)(dbsq)(N_2L)] family, where N_2L = MeO-bpy, bpy, 4,4'-dimethyl-2,2'-bipyridine (Me-bpy), 1,10'-phenanthroline (phen), 2,2'-bipyrimidine (bpym) and 2,2'-bipyrazine (bpyz). The resultant model for VT $T_{1/2}$ prediction is user-friendly, accurate and improves computational-screening approaches.

RESULTS AND DISCUSSION

Synthesis and Experimental Work

To provide a wider range of experimentally reported valence tautomeric $T_{1/2}$ values in toluene for [Co(dbdiox)(dbsq)(N_2L)] complexes for our DFT analysis, we synthesized the complex [Co(dbdiox)(dbsq)(MeO-bpy)] (**1**) (see Supporting Information section 2-4, 6 for more experimental detail, Figure S1-13, Table S1-4). The ancillary ligand MeO-bpy was selected for this work as its relatively poor π-accepting ability is expected to stabilize the LS-Co^{III}-(cat)(SQ) tautomer and increase the $T_{1/2}$ relative to other diimine ligands, based on previous studies that suggest reducing diimine π-acceptance favors the LS-Co^{III}(cat)(SQ) form.[22–24] This allows for the provision of a higher temperature experimental data point for comparison with calculated values (Table S1).

Complex **1** crystallizes as the toluene solvate **1**·2tol and the single crystal X-ray structural analysis at 100 K indicates interatomic distances consistent with the LS-Co^{III}-(cat)(SQ) state (Figure S2). The octahedral *SHAPE* index of 0.414,[60,61] and the Σ and Θ angles of 42° and 125° respectively (calculated by OctaDist),[62] show low distortion of the octahedron characteristic of

LS-Co^{III} (Table S3). Variable temperature crystallography (100–200 K)[63] suggests the onset of VT (Table S3, Figure S5) with increasing temperature. Complex **1** was isolated in bulk as the unsolvated compound, and as partially desolvated **1**·0.8tol, with solvation levels confirmed by elemental analysis and thermogravimetric analysis in each case (Figure S1). Infrared (IR) and solid-state ultra-violet-visible (UV-vis) diffuse reflectance spectroscopy (Figure S7, S8) are consistent with **1** and **1**·0.8tol being predominantly in the LS-Co^{III}-(cat)(SQ) state at room temperature (see Supporting Information section 6 for more detail).[23,58,64,65] The solid-state magnetic susceptibility behavior of **1**·0.8tol and **1** indicate both undergo incomplete thermally-induced VT transition, with **1** displaying a more complete transition at 330 K (~38%, based on the maximum $\chi_M T$ value of 2.35 cm^3 mol^{-1} K measured for [Co^{II}(dbsq)$_2$(phen)] in toluene[66]) compared to **1**·0.8tol (~25%) (Figure 1).

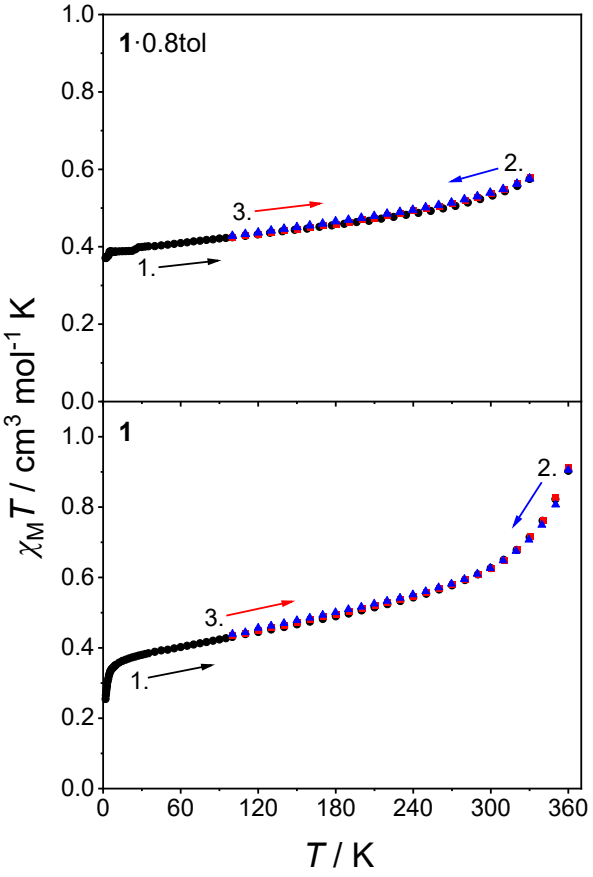

Figure 1. Plot of $\chi_M T$ for solid state **1**·0.8tol (top) on first heating 1.9–330 K (black ●), first cooling 330–100 K (red ■), second heating 100-330 K (blue ▲). Plot of $\chi_M T$ for solid state **1** (bottom) on first heating 1.9–360 K (black ●), first cooling 360–100 K (red ■), second heating 100–360 K (blue ▲). Numbered arrow indicates the order and direction of measurements.

Variable temperature UV-vis absorption spectra of **1** in toluene (Figure 2) reveal intensity changes of bands at ~600 and ~770 nm with temperature. Previous studies have noted that the ~600 nm band is characteristic of the LS-Co^{III}-(cat)(SQ) tautomer and the ~770 nm band is associated with the HS-Co^{II}-(SQ)$_2$ tautomer.[23] Upon heating from 278 to 318 K, the ~ 600 nm band decreases in intensity and the ~770 nm band increases, consistent with the behavior of

literature analogues.[23] These changes are reversible on repeated heating and cooling cycles (Figure S11) and isosbestic points are evident at ~495 and ~660 nm. This behavior is indicative of thermally-induced VT occurring in toluene.[21,23,66] The $T_{1/2}$, ΔH and ΔS values associated with this thermal interconversion were obtained by fitting the HS-Co^{II}-$(SQ)_2$ mole fraction vs the temperature (T) data (Figure S13) to the regular solution mode[67] (See Supporting Information section 1 for more detail). The model provides an excellent fit (R^2 = 1.00) and affords the values: $T_{1/2}$ = 336(1) K; ΔH = 68(2) kJ mol^{-1} and ΔS = 203(6) J K^{-1} mol^{-1}. The $T_{1/2}$ of **1** in toluene is one of the highest reported,[23] extending the range of VT transition temperatures in the [Co(dbdiox)(dbsq)(N_2L)] family, consistent with an electron-rich ancillary ligand.

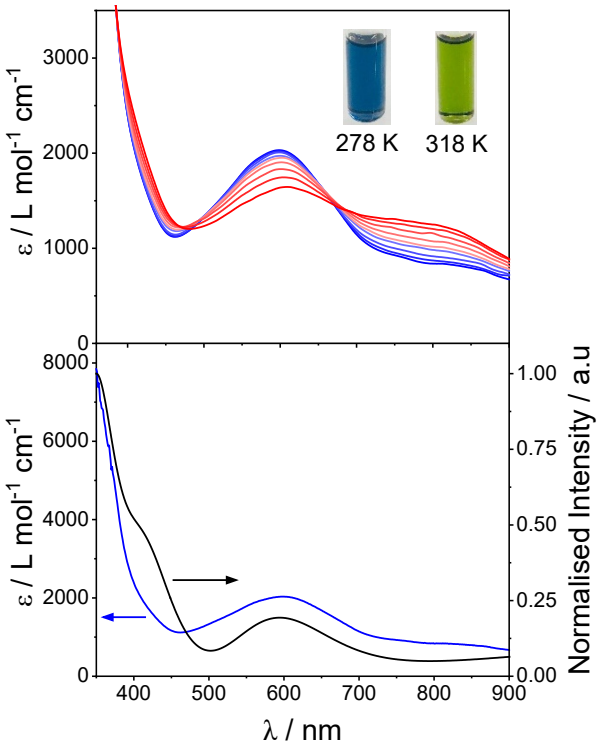

Figure 2. (Top) Variable temperature UV-Vis spectra of **1** in toluene from 278 K (blue) to 318 K (red) in 5 K intervals and photograph of **1** in toluene at these temperature temperatures (inset). (Bottom) Electronic absorption spectra for **1** in toluene: experimental data at 278 K (blue) and curve calculated for the LS-Co^{III}-(cat)(SQ) tautomer with TDA-CAM-B3LYP/def2-TZVPP with a toluene continuum solvation model (black).

Linear-response time-dependent DFT calculations within the Tamm-Dancoff Approximation (TDA-DFT)[68] were used to simulate the electronic absorption spectra for **1** in both the LS-Co^{III}-(cat)(SQ) and HS-Co^{II}-$(SQ)_2$ tautomeric states (Figures S14-S16).[68] These DFT calculations were performed using ORCA (see Supporting Information section 1 for more information).[69,70] The popular global-hybrid functional B3LYP[71,72] is commonly used to simulate spectra,[35,41,72–74] despite its incapability of describing charge transfer (CT) transitions and its

tendency to simulate artificial states instead.[36,75–78] Therefore, to account for CT transitions, range-separated hybrid or double hybrid density functionals should be employed for accurate TDA-DFT excitation energies.[77,79] We found that CAM-B3LYP[80] was the most appropriate method to simulate the spectra for both tautomeric forms of **1** after cross-validation with B3LYP and ωB97X[81] to rule out any potential artifacts (detailed in Supporting Information section 5, Figure S14, S15).

CAM-B3LYP performed very well in reproducing the spectrum of the LS-Co^{III}-(cat)(SQ) form of **1** (Figure 2). The band around 600 nm that is characteristic of the LS-Co^{III}-(cat)(SQ) tautomer, can now be definitively assigned as a localized semiquinonate $\pi \rightarrow \pi^*$ transition (Figure S17). The band at 304 nm observed experimentally (Figure S9) is a ligand-to-metal charge transfer (LMCT) from the $dbcat^{2-}$ to the LS-Co^{III} e_g* orbital (Figure S18). The bands toward the near-infrared (NIR) region (Figure S9) are ($dbcat^{2-} \rightarrow dbsq^{\bullet-}$) intervalence charge transfer (IVCT) bands as previously suggested (Figure S19),[32,66] which disappear as expected in the calculated spectra of the HS-Co^{II}-$(SQ)_2$ state for **1** (Figure S16). As the temperature is increased and **1** interconverts from LS-Co^{III}-(cat)(SQ) to HS-Co^{II}-$(SQ)_2$, the calculated semiquinonate $\pi \rightarrow \pi^*$ band around 600 nm splits into two bands (as there are two independent $dbsq^{\bullet-}$ ligands) (Figure S16, S20, S21), with the experimentally observed band at ~770 nm (Figure 2), which is considered characteristic of HS-Co^{II}-$(SQ)_2$, attributed to one of these transitions with blue-shifting apparent in the calculated spectrum.[82,83] This blue-shifting is known for range-separated hybrids but is generally not a problem due to their ability to describe CT.[77] Additionally, the LMCT band evident for LS-Co^{III}-(cat)(SQ) is replaced by a metal-to-ligand charge transfer (MLCT) transition between the Co^{II} e_g orbital and the $dbsq^{\bullet-}$ π^* (Figure S16, S22), and results in the appearance of a third isosbestic point at ~385 nm (Figure S23). The assignment of the transitions (Table S5) using TDA-DFT confirm

the identity of the characteristic tautomeric bands for the [Co(dbdiox)(dbsq)(N_2L)] family of complexes, which up to now have only remained speculative.[23,32,66]

Density Functional Theory Calculations

A pioneering DFT study on the VT complex [Co(dbdiox)(dbsq)(phen)] was reported by Noodleman, Hendrickson *et al*. in 1997.[27] This study investigated electronic structures, energy differences and vertical optical transition energies for the LS-Co^{III}-(cat)(SQ), LS-Co^{II}-$(SQ)_2$, and HS-Co^{II}-$(SQ)_2$ electromers using (semi-)local density functional calculations on the molecular crystal structure with *tert*-butyl groups replaced by hydrogen atoms. This phenanthroline compound is notable in that crystallographic data exist for both valence tautomeric forms.[23] These calculations confirmed a LS-Co^{III}-(cat)(SQ) ground state but predicted the experimentally unobserved LS-Co^{II}-$(SQ)_2$ tautomer to be next lowest in energy. The decreased $T_{1/2}$ for [Co(dbdiox)(dbsq)(phen)] compared to other analogues was attributed to increased π-backbonding involving the phenanthroline ligand.

Given the tremendous advances in computational chemistry in the last twenty years, we sought to develop and apply accurate DFT to the whole [Co(dbdiox)(dbsq)(N_2L)] family of complexes with the goals of reproducing the spin density distributions and energies of the tautomeric forms, as well as the $T_{1/2}$ values for the analogues that display VT. Again, we performed all DFT calculations in ORCA (see Supporting Information section 1 for more information).[69,70] To develop the model we investigated the [Co(dbdiox)(dbsq)(N_2L)] complexes where N_2L = MeO-bpy, Me-bpy, bpy, phen, bpym, and bpyz, which offer a wide $T_{1/2}$ (toluene) range of 190–336 K (Table S1).[21,23,27,66,84] Solution state transition temperatures were employed due to the complications of solid state and packing effects associated with solid state values,[23,58,59] with toluene providing the most comprehensive set of experimental values. The analogue with the 4,4'-

diphenyl-2,2'-bipyridine ancillary ligand displays unexplained anomalous behavior, with the experimentally observed $T_{1/2}$ very high for the ΔH and ΔS values, and was not included.[23,66]

Density functional for geometry optimizations

To produce chemically accurate results, reliable DFT optimized geometries, and proper electronic descriptions, it is important to carefully select the functional and atomic orbital basis set. As [Co(dbdiox)(dbsq)(N_2L)] complexes possess open-shell electronic configurations in both tautomeric states, obtaining correct geometries and spin-density distributions, though difficult, is crucial. We chose the [Co(dbdiox)(dbsq)(phen)] complex to trial DFT geometry optimization as there are crystal structures for both tautomeric forms.[23] The LS-Co^{III}-(cat)(SQ) tautomeric form contains localized singlet catecholate and doublet semiquinonate ligands according to crystallographic information (Figure S2).[21,23] However, this localized unpaired electron can easily leak across the two dioxolene ligands during geometry optimization due to the common self-interaction error (SIE),[85–88] an effect where the electrons display unphysical interaction with themselves. Selection of a density functional that prevents such artificial delocalization of the spin density is vital, something not properly considered in the literature despite knowledge of this problem, with methods applied that did not localize the spin.[27,28,32,35,89] In general, generalized gradient approximations (GGA) functionals, such as BP86,[90,91] give reliable geometries and are widely used in many computational studies including for valence tautomeric cobalt complexes.[35,39,92] However, for [Co(dbdiox)(dbsq)(phen)], the BP86 functional results in delocalized spin distribution in the doublet LS-Co^{III}-(cat)(SQ) tautomer resulting from high amounts of SIE (Figure 3). The 2010 study by Yoshikawa *et al.* employed B3LYP, B3LYP*,[93] BLYP,[90,94] BP86 and OPBE[91,95] to obtain the relative energy of the VT process and Co–O bond

lengths.[28] The best-performing functional in their study, B3LYP*, still had significant SIE resulting in an equal distribution of spin densities among the two dioxolene ligands (Mulliken spin densities of 0.47 for both $dbcat^{2-}$ and $dbsq^{\bullet-}$).

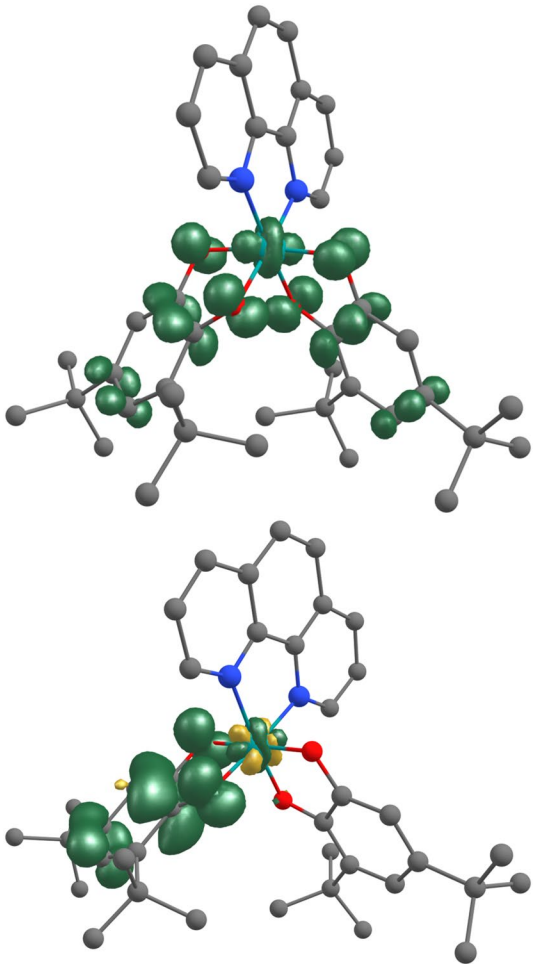

Figure 3. Optimized geometry and spin density distribution of [Co^{III}(dbcat)(dbsq)(phen)] as calculated by BP86-D3(BJ)/def2-TZVPP (top) and PBEh-3c (bottom). The spin distribution represents positive (green) and negative (yellow) spin densities with isovalue=0.004. Hydrogen atoms omitted for clarity.

We found that the efficient hybrid functional PBEh-3c,[96] which includes a London dispersion correction,[97,98] a specialized double-ζ basis set to reduce incompleteness effects whilst still being computationally efficient, and a fast basis set superposition error correction,[99] performed extremely well in producing the accurate geometry with the desired spin distribution for the LS-Co^{III}-(cat)(SQ) (Figure 3, Figure S25), as well as HS-Co^{II}-$(SQ)_2$ (S = 5/2, 3/2, 1/2) states in [Co(dbdiox)(dbsq)(phen)] (Figure S25, S29). The admixture of Fock exchange in PBEh-3c explains the reduction of the SIE and the resulting localization of the spin density. To further minimize errors associated with the LS-Co^{III}-(cat)(SQ) form, we generated all input coordinates for the geometry optimizations for each complex using the LS-Co^{III}-(cat)(SQ) crystal structure for **1** and [Co(dbdiox)(dbsq)(phen)][23] as the template. The calculated LS-Co^{III}-(cat)(SQ) structure for **1** matched the crystal structure well (Figure S5). The antiferromagnetic (S = 3/2, S = 1/2) states for HS-Co^{II}-$(SQ)_2$ can be obtained using the broken-symmetry (BS) approach,[100] but subsequent inspection of the spin densities is mandatory as the BS approach does not guarantee the desired spin-states. We therefore ensured each state had the desired spin orientation by analyzing the spin density plots and spin-populations of all complexes before further calculations (Figure S26-S31).

Density functional study for spin-state energetics

We set about calculating the spin-state energies of each tautomeric state for the [Co(dbdiox)(dbsq)(N_2L)] family, with the aim of exploring a possible correlation between the energy difference between tautomers with the experimentally observed $T_{1/2}$. As the spin-state energy is a crucial piece of information in VT complexes, obtaining accurate and quantitative

descriptions is paramount. We therefore performed a detailed functional benchmarking study on [Co(dbdiox)(dbsq)(phen)] and [Co(dbdiox)(dbsq)(bpy)], chosen as they contain "parent" diimine ancillary ligands that have been chemically derivatized in the other analogues. We included a suite of corrections to ensure greatest approximation of reality in the calculations of the electronic energy (E_e) of each tautomer. Each tautomer was calculated with dispersion corrections to account for ubiquitous London dispersion interactions, zeroth order regular approximation (ZORA)[101] relativistic corrections, with the relativistic equivalent of the def2-TZVPP basis set,[102] the conductor-like polarizable (CPCM) solvent model[103] with toluene as the solvent. Additionally, the zero-point, and thermal vibrational contributions (calculated with PBEh-3c) at the corresponding transition temperatures of each complex (Table S6) were also included. With these effects included, we trialed the following eight different DFT methods to calculate the spin-state energies for [Co(dbdiox)(dbsq)(phen)] and [Co(dbdiox)(dbsq)(bpy)] and, most importantly, compared the calculated values with the experimentally determined enthalpy change (26.77 and 36.56 kJ mol^{-1} respectively)[23,66] for the VT interconversion (ΔH) (Table S7):

- Generalized gradient approximation (GGA) functionals: BP86, OPBE, B97M[104] (B97M-V parametrization but paired with different dispersion corrections; see below)[105,106]
- Meta-GGA functional: M06-L[107]
- Global hybrid functionals (admixture of Fock exchange given in parentheses): B3LYP (20%), TPSSh (10%)[108]
- Long-range corrected hybrid functionals: ωB97X[109] (ωB97X-V parametrization but paired with different dispersion corrections; see below)[105,106]
- Global Double-hybrid functional: B2PLYP[110] (consisting of 27% MP2 correlation and 53% admixture of Fock exchange)

As the electronic energy with the relevant thermal corrections (ΔE_t) can be related to the enthalpy, where $\Delta H = \Delta E_e + \Delta E_t$,[27,111] the electronic energies obtained for each state was supplemented with the relevant thermal corrections (including zero point and thermal vibrational effects) obtained from the frequency analysis with PBEh-3c geometries (Figure S28, S29, Table S6). Most previous studies on VT and SCO complexes have neglected dispersion corrections to allow for an improved description of intermolecular forces.[5,27,28,35,44,46,49] We used dispersion-corrected DFT in our study to mimic reality as much as computationally possible. We combined the eight functionals with the extensively used DFT-D3 model, with the Becke and Johnson damping scheme DFT-D3(BJ) (except M06-L which used the zero-damping scheme DFT-D3(0)),[98,112] and the newly implemented DFT-D4 correction which introduces correction for atomic charge and spin-states (Table S7).[113,114] This results in a total of sixteen different dispersion-corrected DFT methods trialed, one of the widest study reported for VT or SCO switchable molecules.

In benchmarking each method to [Co(dbdiox)(dbsq)(bpy)] and [Co(dbdiox)(dbsq)(phen)], we found that the BP86 and OPBE functional with both dispersion corrections overstabilized the LS-Co^{III}-(cat)(SQ) state, and the B3LYP and ωB97X functionals (both dispersion corrections) incorrectly favored HS-Co^{II}-$(SQ)_2$ as the ground state (Table S7). The inability to accurately produce the ground state using B3LYP and the overstabilization of the LS-Co^{III}-(cat)(SQ) tautomer using BP86 is consistent with previous work.[39] The B2PLYP, TPSSh and B97M functionals performed moderately with a mean absolute error (MAE) of ~20 kJ mol^{-1} from the experimental values for both dispersion corrections (Figure 4, Table S7). The OPBE and TPSSh functionals, which are extensively used in spin-state energy studies without dispersion corrections, are noted to differ in their performance with the two different dispersion correction models (Figure 4, Table

S7). Compared to OPBE calculated without dispersion corrections, the MAE of OPBE calculated with both dispersion corrections increased by 40–60 kJ mol^{-1}, indicating the performance of the uncorrected functional is attributed to error compensations. Of all the methods used, the M06-L-D4 approach showed outstanding performance, with a MAE of only ~1 kJ mol^{-1} (0.25 kcal mol^{-1}) (Figure 4, Table S7). We found that the calculated energies using M06-L-D3(0) did not change significantly (Table S7), unlike observed with OPBE and TPSSh, indicating that there is no error compensation associated within the functional. The excellent match between experimental and calculated values for the complexes with bpy and phen supports M06-L-D4 as the most appropriate computational method to apply to the whole [Co(dbdiox)(dbsq)(N_2L)] family.

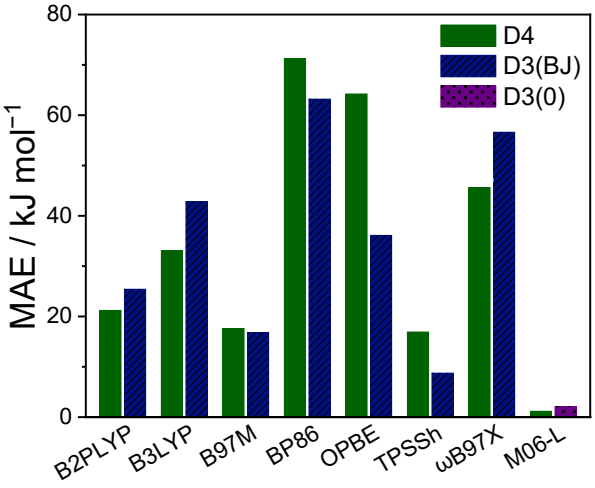

Figure 4. Mean absolute error (MAE) for functional screening for spin-state energetics of [Co(dbdiox)(dbsq)(bpy)] and [Co(dbdiox)(dbsq)(phen)] complexes with the DFT-D4, -D3(BJ) or -D3(0) dispersion corrections.

A common practice to save computational time in computational treatments is to truncate structures by removing large functional groups. To date, major computational studies on the [Co(dbdiox)(dbsq)(N_2L)] VT system have been performed with replacement of the *tert*-butyl groups with hydrogen atoms or with methyl groups.[27,28,32] This approach is not recommended as it alters the energy preference of the states,[37] and some of us have shown that the *tert*-butyl groups can have a significant effect on the relative tautomer energies.[39] Calculation of **1** with all *tert*-butyl groups removed with M06-L-D4 gave ΔH value of 33.5 kJ mol^{-1}, a significant deviation from the experimental values of 68 kJ mol^{-1}, highlighting that truncation should not occur if accurate spin-state energies are required. We therefore performed all calculations with the *tert*-butyl groups in place. With the *tert*-butyl groups present, there are four possible geometric isomers for the LS-Co^{III}-(cat)(SQ) tautomer of which only three isomeric forms are observed in the solid-state (Chart S1).[21,23,24] We found that the isomers have slight differences in energy (Table S8). However, as isomer-1 (Chart S1) is the lowest in energy for both tautomers for **1**, as well as being the most observed in the solid state across all complexes,[21,23,24] we have chosen to perform all our calculations on this isomer with coordinates generated from the LS-Co^{III}-(cat)(SQ) form of the phen and MeO-bpy complexes. We applied the best performing M06-L-D4-ZORA/def2-TZVPP(CPCM) to calculate the energies of all compounds in the [Co(dbdiox)(dbsq)(N_2L)] family (Table 1, Table S9). The M06-L-D4-ZORA/def2-TZVPP(CPCM) method accurately matches the calculated and experimentally determined enthalpies for all complexes, with a MAE of just 3.6 kJ mol^{-1} (< 1 kcal mol^{-1}) and a maximum error of only 9 kJ mol^{-1} (2.2 kcal mol^{-1}) (Table 1) lying well within the chemical-accuracy threshold for computational thermochemistry and spin-state energetics.[39]

Table 1. Calculated ΔH for the [Co(dbdiox)(dbsq)(N_2L)] family M06-L-D4-ZORA/def2-TZVPP(CPCM) method with toluene.

N_2L	$T_{1/2}$ / K[b]	$\Delta H_{VT\text{-}interconversion}$ / kJ mol^{-1}		Error / kJ mol^{-1}
		Calculated	Experimental	
MeO-bpy	336(1)[a]	58.53	68[a]	9.47
Me-bpy[23]	292	35.86	38.36	2.5
bpy[23]	275	34.86	36.56	1.7
phen[23]	228	27.37	26.77	-0.6
bpym[23]	190	27.72	-	-
bpyz[23]	<190	24.75	-	-

[a]Reported in this work. [b]$T_{1/2}$ is the temperature where there are equal populations of the LS-Co^{III}-(cat)(SQ) and HS-Co^{II}-$(SQ)_2$ tautomers.

The $T_{1/2}$ (toluene) values of the [Co(dbdiox)(dbsq)(N_2L)] complexes increase with both experimental and calculated ΔH (Table 1). We expected that a model correlating the calculated ΔH with the experimentally determined $T_{1/2}$ (toluene) of the complexes could provide a predictive tool for targeted synthesis of VT compounds, with the correlation indeed producing a moderate fit (Figure S32).[23,27,66,84] However, the calculations are computationally expensive, and so we explored the possibility of a simpler and faster alternative method based only on calculating properties of the ancillary diimine ligands.

Ancillary ligand effect

The diimine ancillary ligand in the [Co(dbdiox)(dbsq)(N_2L)] complexes clearly controls the charge distribution, possibility of a VT interconversion, and the transition temperature. Experimental data for these complexes suggest that the $T_{1/2}$ increases as the reduction potential (E_{red}) of the ancillary diimine ligand decreases.[22,23] This relationship has been postulated to occur based on the ability of

the lowest unoccupied molecular orbital (LUMO) of the ancillary ligand to stabilize the electron-rich HS-Co^{II} center via π-backbonding.[5,23,27] However, there is also the potential for the diimine highest occupied molecular orbital (HOMO) to stabilize the electron-poor LS-Co^{III} center via σ-donation. A synergistic σ-donating/π-accepting effect could also be involved in tuning the $T_{1/2}$ value. We noticed the Hammett parameters for the ring substituents in MeO-bpy, Me-bpy and bpy correlate with the $T_{1/2}$ (toluene) for the corresponding complex (Figure S33), further suggesting the role of π-backbonding and/or σ-donation.[23,115,116] To provide a simpler ligand-based model to predict $T_{1/2}$, we wanted to determine unequivocally if one effect dominates, or if there is equal π-backbonding/σ-donating effects.

To study the effect of the N_2L ancillary ligand, it is crucial to understand the electronic configuration and ligand-field splitting of the cobalt center in both the LS-Co^{III}-(cat)(SQ) and HS-Co^{II}-$(SQ)_2$ tautomers. As the complexes are open shell in both tautomeric states, both the spin up (α) and spin down (β) orbitals in unrestricted calculations need to be considered. The electronic configurations of the LS-Co^{III}-(cat)(SQ) and HS-Co^{II}-$(SQ)_2$ forms in quasi-octahedral symmetry are $(t_{2g})^6(e_g^*)^0(\pi^*cat)^2(\pi^*sq)^1$ and $(t_{2g})^5(e_g^*)^2(\pi^*sq_1)^1(\pi^*sq_2)^1$ respectively.[27,66] The idealized spin splitting diagram of the cobalt center (Figure S34, Table S10) has a $(d^3\alpha)(d^3\beta)$ occupation for LS-Co^{III} and $(d^5\alpha)(d^2\beta)$ for HS-Co^{II}.

To ascertain the extent of σ-donation and π-backbonding ancillary ligand effects, we calculated the HOMO and LUMO energies for each complex in both tautomeric forms (Table S11). For this discussion, as the MeO-bpy and bpyz containing complexes represent the two extreme cases (highest and lowest $T_{1/2}$ respectively), the LS-Co^{III}-(cat)(SQ) tautomer in **1** and the HS-Co^{II}-$(SQ)_2$ tautomer in [Co(dbdiox)(dbsq)(bpyz)] are discussed. For **1**, the HOMO (both α and β) is located on the Co^{III}-(cat) moiety (Figure 5). The α LUMO is localized on the MeO-bpy ligand,

allowing for potential π-backbonding with the LS-Co^{III} center, whilst the β LUMO is concentrated on the Co^{III}-(SQ) moiety and can thus be stabilized via σ-donation from the lower lying MeO-bpy occupied orbitals. In [Co^{II}(dbsq)$_2$(bpyz)], both the α and β LUMO are localized on the bpyz ligand and both α and β HOMO are concentrated on the HS-Co^{II}-$(SQ)_2$ moiety (Figure 5). Both the α and β HOMOs of [Co(dbsq)$_2$(bpyz)] can be stabilized via π-backbonding interactions with the bpyz LUMO. This shows that the LS-Co^{III}-(cat)(SQ) form has potential for both π back bonding and σ-donation whilst the HS-Co^{II}-$(SQ)_2$ tautomer is predominantly stabilized by π-backbonding.

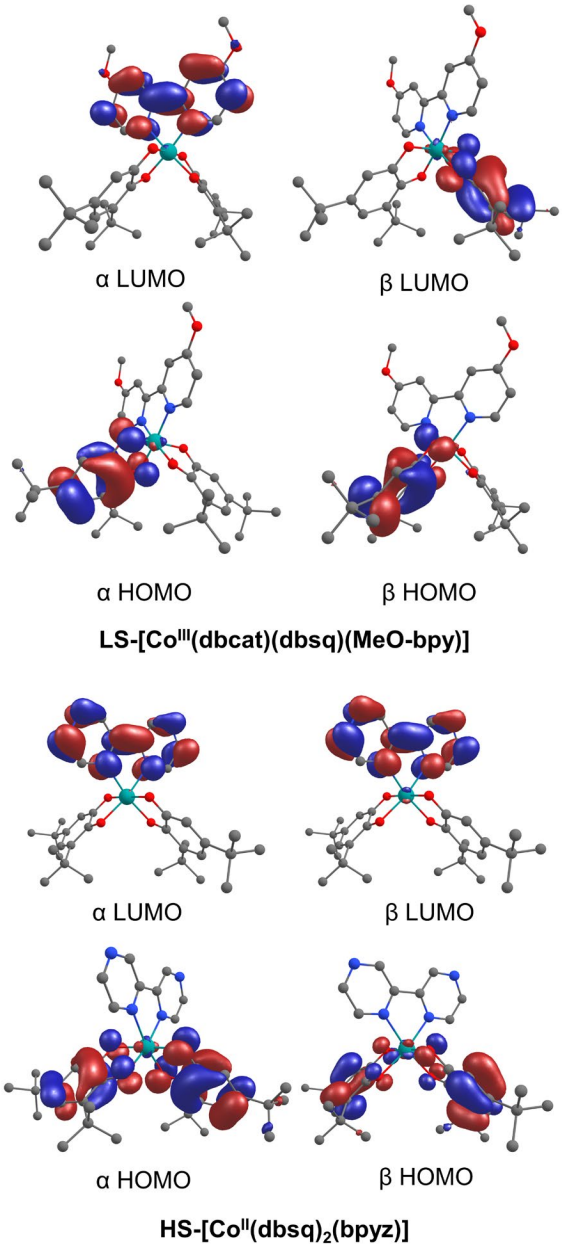

Figure 5. HOMO and LUMO of LS-Co^{III}-(cat)(SQ) tautomer of **1** representing energies of corresponding α and β orbitals (top) and HOMO and LUMO of HS-Co^{II}-$(SQ)_2$ tautomer of [Co(dbdiox)(dbsq)(bpyz)] representing energies of corresponding α and β orbitals (bottom) calculated using PBEh-3c (gas phase).

The HOMO and LUMO (α and β) for both tautomeric forms of all the studied complexes were calculated (Figure 6, Figure S35-38). The trend where the α and β HOMOs of the HS-Co^{II}-$(SQ)_2$ tautomer (stabilized via π-backbonding) (Figure S37) and β LUMO of LS-Co^{III}-(cat)(SQ) tautomer (stabilized via σ-donation) (Figure S36) are localized on the Co-diox moiety is noted across all complexes. Interestingly, the β LUMO of HS-Co^{II}-$(SQ)_2$ shifts from the Co-diox moiety toward the N_2L ligand moving from MeO-bpy to bpyz (Figure 6), following the trend of increased π-acceptance. From the orbital analysis, the bpyz ligand more strongly stabilizes HS-Co^{II}-$(SQ)_2$ via π-interactions compared to MeO-bpy, explaining the decrease in the measured $T_{1/2}$ values.

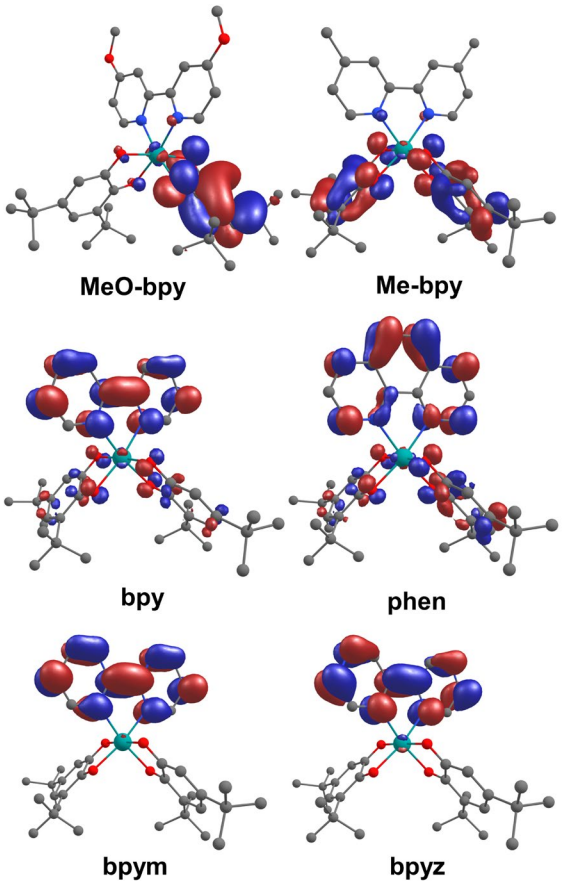

Figure 6. LUMO (β) of HS-Co^{II}-$(SQ)_2$ tautomer of [Co(dbdiox)(dbsq)(N_2L)] (N_2L = MeO-bpy, Me-bpy, bpy, phen, bpym, bpyz) calculated using PBEh-3c (gas phase). LUMO is seen shifting from the HS-Co^{II}-$(SQ)_2$ moiety to the ancillary ligand as it moves from MeO-bpy to bpyz (changes in the orbital ordering), accommodating increased π-backbonding capabilities.

We proceeded to systematically analyze the energy levels of the HOMO and LUMO (average of α and β) for each complex in both tautomeric forms (Table S11). We observed that the HOMO of the HS-Co^{II}-$(SQ)_2$ tautomer has been stabilized compared to the HOMO of the LS-Co^{III}-(cat)(SQ) form (Figure 7) (average 165 kJ mol^{-1} stabilization), most likely resulting from π-backbonding with the N_2L ligand. The LUMO of the LS-Co^{III}-(cat)(SQ) tautomer has also been

stabilized compared to the LUMO of the HS-Co^{II}-$(SQ)_2$ form (average 55 kJ mol^{-1} stabilization), arising from increased σ-donation effects (Figure 7). However, the stabilization of the HS-Co^{II}-$(SQ)_2$ HOMO is three times greater compared to the stabilization of the LS-Co^{III}-(cat)(SQ) LUMO across the entire series (Figure 7), indicating that diimine π-backbonding effects lower the energy of the HOMO to a greater extent compared to the lowering of the LUMO energy via σ-donation. The diimine influence on the $T_{1/2}$ can be considered as arising from 75% π-acceptance and 25% σ-donation. To evaluate the relationships between the ancillary ligand bonding and the experimental $T_{1/2}$ values, the $T_{1/2}$ for each complex (excluding bpyz where the $T_{1/2}$ is not precisely known) was plotted against the LS-Co^{III}-(cat)(SQ) LUMO and HS-Co^{II}-$(SQ)_2$ HOMO energies (Figure S39). Both plots show a positive linear correlation, corresponding to stabilization from σ-donation and/or π-acceptance. However, the correlation is slightly more prominent for the HS-Co^{II}-$(SQ)_2$ HOMO, confirming that π-acceptance is the dominant effect. Thus, it was determined that both N_2L σ-donation and π-backbonding influence the transition temperature in [Co(dbdiox)(dbsq)(N_2L)] complexes, but with π-acceptance significantly dominating. A more electron-rich N_2L diimine ligands will stabilize the LS-Co^{III}-(cat)(SQ) tautomer and increases the transition temperature.

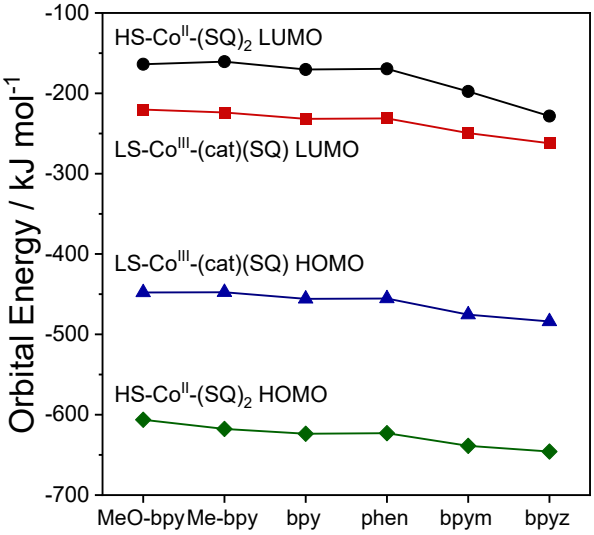

Figure 7. HOMO and LUMO energies (average of α and β manifolds) of LS-Co^{III}-(cat)(SQ) and HS-Co^{II}-(SQ)$_2$ tautomers for [Co(dbdiox)(dbsq)(N$_2$L)] (N$_2$L = MeO-bpy, Me-bpy, bpy, phen, bpym, bpyz) calculated with PBEh-3c in gas phase.

Predicting Valence Tautomeric Transition Temperature

From the conclusion that the π-accepting ability of the diimine ligand dominates in influence over the transition temperature in the [Co(dbdiox)(dbsq)(N$_2$L)] complexes, we hypothesized that the LUMO energy of the diimine ligand should correlate with the $T_{1/2}$ for analogues that undergo VT. If so, this would provide a route to a simple model to predict the transition temperature of [Co(dbdiox)(dbsq)(N$_2$L)], where only the orbital energies of the diimine ligand would need to be calculated. Accordingly, we set about calculating the LUMO and HOMO energies for each ancillary ligand (MeO-bpy, Me-bpy, bpy, phen, bpym, bpyz) in this study.

To ensure that our results are not method or model dependent, we tested the PBEh-3c functional, the double hybrid B2PLYP (where the orbitals are a result of self-consistent field (SCF)

calculations with the hybrid component of B2PLYP), and the Hartree-Fock (HF) method to calculate the HOMO and LUMO energies of each individual N_2L ligand in both the gas phase and in toluene. The calculated energies (each method) of the HOMO, LUMO as well as the HOMO-LUMO gap for each ligand were plotted against the experimentally determined $T_{1/2}$ for the corresponding complex (Figure S40-S42).[23,27,66,84] Ligand bpyz was excluded from the plots as the $T_{1/2}$ of the complex is not definitively known.[23] We observed a strong positive correlation between the LUMO energy of the diimine ligands and the experimental $T_{1/2}$ values for all methods in both toluene and the gas phase, with high R^2 values ranging from 0.91 to 0.96 (Table 2, Figure S40), as predicted. Plotting the diimine HOMO or HOMO-LUMO gap energy vs the $T_{1/2}$ does not produce a meaningful correlation for every method in both the gas and solution phases (Figure S41, S42, Table S12) to be expected as π-backbonding dominates. A strong correlation between the HOMO energy of HS-Co^{II}-$(SQ)_2$ tautomer for each complex and LUMO energy of the corresponding diimine ligands (Figure S43) indicate that the diimine LUMO π-backbonds with the HS-Co^{II}-$(SQ)_2$ HOMO. Previous work has shown that the LUMO+1 of phenanthroline-based ligands predominantly undergoes π-backbonding with the metal center, rather than the LUMO.[5,117–119] However, as the LUMO and LUMO+1 for phenanthroline are effectively degenerate, plotting the phenanthroline LUMO will achieve the same result.[5] A simple correlative model to predict VT transition temperature in [Co(dbsq)(dbdiox)(N_2L)] complexes has been achieved.

Table 2. Average deviation between the predicted and experimental $T_{1/2}$ for [Co(dbdiox)$_2$(N$_2$L)] (N$_2$L = MeO-bpy, Me-bpy, bpy, phen, bpym) complexes calculated with different methods

Method	R^2	MAE between predicted and experimental $T_{1/2}$ / K[a]	Average % error
PBEh-3c (gas phase)	0.96	11	4.2%
PBEh-3c (toluene)	0.95	12	4.9%
B2PLYP[b] (gas phase)	0.94	15	5.9%
B2PLYP[b] (toluene)	0.93	13	5.2%
HF[b] (gas phase)	0.91	24	9.4%
HF[b] (toluene)	0.93	22	8.5%

[a]Experimentally determined $T_{1/2}$ measured in toluene. [b]Calculated with def2-TZVPP basis set

To determine the accuracy and predictive power of the six correlative models between the diimine LUMO and the complex $T_{1/2}$, we used each method (PBEh-3c, B2PLYP and HF) and phase (gas or toluene) to 'predict' the $T_{1/2}$ of each complex using the LUMO energy of the ancillary ligand. For each method and phase, we produced five plots, with each plot having one ligand removed (e.g. bpy), with the resulting plot used to predict the $T_{1/2}$ of the missing ligand complex (e.g. [Co(dbdiox)(dbsq)(bpy)]) (Table S13). This level of benchmarking is not matched by any previous DFT studies of SCO or VT compounds. The MAE of the predicted $T_{1/2}$ values from each method compared with experimental $T_{1/2}$ values (Table 2) is low across all methods and phases. These low errors validate the accuracy of this method to correlate the diimine LUMO energy and $T_{1/2}$ value. The most accurate functional, PBEh-3c, affords an excellent match between calculated and experimental $T_{1/2}$ values, with only 4.2% and 4.9% average error for gas phase and toluene, respectively (Table 2).

The simple model we present here for the [Co(dbdiox)(dbsq)(N$_2$L)] complexes, correlating calculated diimine LUMO energy ($E_{\text{Ligand-LUMO}}$, kJ mol^{-1}) (PBEh-3c, gas phase) with experimentally determined $T_{1/2}$ values in toluene, will allow accurate prediction of the likelihood

of VT and the approximate $T_{1/2}$ value for new analogues in his family (Figure 8).[23,27,66,84] The transition temperature is easily calculated using $T_{1/2} = 1.87 \times E_{\text{Ligand-LUMO}} + 419$. Calculation of the LUMO of a proposed diimine ancillary ligand is computationally simple and fast, allowing for rapid ligand screening. Examination of the recent literature suggest that our method is valid for systems with more elaborate functionalization of the diimine ligands. A recently reported [Co(dbdiox)(dbsq)(N_2L)] VT complex incorporates the ethyl-ester phenanthroline derivative (with *para*-phenylene as a spacer) Phen-COOEt (Chart S2) as the diimine ligand, with the aim of grafting the complex on metal oxide surfaces.[32] Calculations of the LUMO and LUMO+1 energy levels of Phen-COOEt using PBEh-3c (gas) yielded values of −123 and −102 kJ mol^{-1} respectively. Application of our method (Figure 8) affords a predicted $T_{1/2}$ of 228 K for the complex using the Phen-COOEt LUMO+1 energy, as the LUMO and LUMO+1 are not degenerate.[5,117–119] This is an excellent match with the experimental $T_{1/2}$ value of 230 K in toluene,[32] demonstrating the remarkable predictive power of our method, even with more elaborate functional groups on the ancillary ligand. Including Phen-COOEt, the average error between the predicted and experimental $T_{1/2}$ values determined using the correlation shown in Figure 8 for the six N_2L ligands (MeO-bpy, Me-bpy, bpy, phen, bpym, Phen-COOEt) is only 3.7%. The LUMO+1 and $T_{1/2}$ for Phen-COOEt and the corresponding complex can be added to Figure 8 (Figure S44) and illustrates the ability to continually add to this model as more experimental data points are generated.[23,27,66,84]

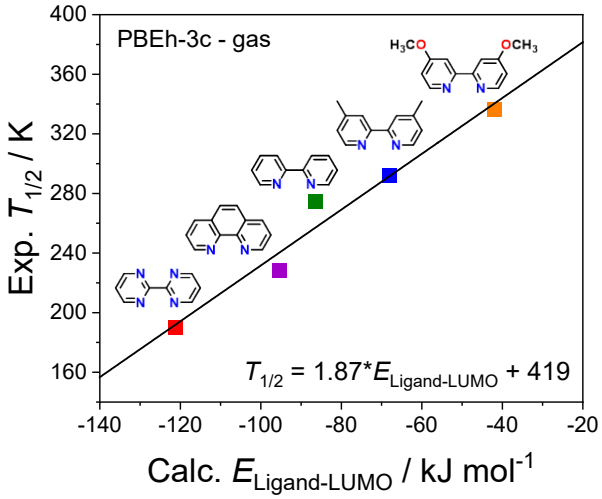

Figure 8. Correlation of the experimentally determined $T_{1/2}$ values for [Co(dbdiox)(dbsq)(N_2L)] (where N_2L = bpym, phen, bpy, Me-bpy, or MeO-bpy) complexes in toluene with the calculated LUMO energy of the N_2L ligand (kJ mol^{-1}) using PBEh-3c (gas phase). Inset: linear equation for $T_{1/2}$ (K) and $E_{Ligand-LUMO}$ (energy (E) of the N_2L LUMO, kJ mol^{-1})). R^2 = 0.96.

Other switchable-molecule families, most commonly Fe(II) SCO systems, display dependence of spin-state on the electron withdrawing/donating nature and/or Hammett-parameters of ligand substituents, and therefore the energy of the ligand LUMO and/or HOMO.[44,49,120–126] We envision that our approach to correlate solution-state $T_{1/2}$ values with calculated ligand LUMO, HOMO or HOMO-LUMO gap energies has great potential to be translated to other valence tautomeric systems with redox-active ligands other than dioxolene. The strategy we report is computationally fast, accurate and not limited to N-donor ligands, in contrast with previous methods that are only applicable to N-donor ligands[43,45,49] or with large experimental/calculated errors and computationally-expensive DFT calculations.[42,44,46,47] As demonstrated with

[Co(dbdiox)(dbsq)(Phen-COOEt)], the developed approach will also not necessarily be restricted to simple substituents with known Hammett parameters.

CONCLUDING REMARKS

We have reported the first accurate electronic descriptions of both the LS-Co^{III}-(cat)(SQ) and HS-Co^{II}-$(SQ)_2$ tautomers for [Co(dbdiox)(dbsq)(N_2L)] VT complexes, which afford precise spin distributions and an excellent match between the calculated and experimental energy separations. All possible effects have been considered in our DFT calculations - solvent model, dispersion corrections, relativistic corrections, thermal corrections, and isomer geometries. The detailed and comprehensive DFT-based protocol reported provides a benchmark for future studies on other switchable molecules and is a significant step forward towards the widespread adoption of computational screening for properties prior to experimental synthesis and analysis.

The effect of the diimine ancillary ligand on the $T_{1/2}$ (toluene) values for the [Co(dbdiox)(dbsq)(N_2L)] family of complexes has been confirmed to originate from a dominant π-accepting effect. This has allowed us to correlate experimentally determined solution-state $T_{1/2}$ values with calculated LUMO energies of the respective diimine ligands. This model affords accurate prediction of $T_{1/2}$ values for [Co(dbdiox)(dbsq)(N_2L)] complexes, with an error of only 3.7%, and allows experimental users to identify potential new diimine ligands that will impart a transition in the desired temperature range. This capability will streamline the development of multifunctional VT complexes and enduing applications. The computationally rapid, accurate and simple approach to correlate ligand-orbital energies with solution transition temperature lays the

foundation for future work to generate models that can be used to predict transition temperature for other switchable molecular systems, helping to expedite routine computer guided synthesis.

ASSOCIATED CONTENT

Supporting Information. The Supporting Information is available free of charge available. Details of experimental and synthetic methods, additional discussion, IR, TGA, crystallography, structural analysis, magnetic measurements, UV-Vis-NIR, TDA-DFT, DFT (PDF)

X-ray crystallographic files for **1**·2tol 100 K (CIF)

1·2tol 150 K (CIF)

1·2tol 200 K (CIF)

DFT optimized XYZ coordinates of complexes (ZIP) and ligands (ZIP)

AUTHOR INFORMATION

Corresponding Authors

Colette Boskovic – *School of Chemistry, University of Melbourne, Parkville, VIC, 3010, Australia*; orcid.org/0000-0002-1882-2139 ; E-mail: c.boskovic@unimelb.edu.au

Lars Goerigk- *School of Chemistry, University of Melbourne, Parkville, VIC, 3010, Australia*; orcid.org/ 0000-0003-3155-675X ; E-mail: lars.goerigk@unimelb.edu.au

Author Contributions

The manuscript was written through contributions of all authors. All authors have given approval to the final version of the manuscript. ‡These authors contributed equally.

Notes

The authors declare no competing financial interest.

ACKNOWLEDGMENTS

C.B. thanks the Australian Research Council for financial support (DP190100854). L.G. is grateful for generous allocations of computational resources from the National Computational Infrastructure (NCI) Facility within the National Computational Merit Allocation Scheme (project fk5) and Research Platform Services (ResPlat) at The University of Melbourne (project punim0094). This research was also supported by the sustaining and strengthening merit-based access to the NCI LIEF Grant (LE190100021) facilitated by The University of Melbourne. F.Z.M.Z acknowledges the Australian Government Research Training Program Scholarship. KSM thanks the Australian Research Council for support (DP170100034). This research was undertaken in part using the MX2 beamline at the Australian Synchrotron, part of ANSTO, and made use of the ACRF detector.

REFERENCES

(1) Mathur, N. Nanotechnology: Beyond the Silicon Roadmap. *Nature* **2002**, *419*, 573–575.

(2) Wasielewski, M. R.; Forbes, M. D. E.; Frank, N. L.; Kowalski, K.; Scholes, G. D.; Yuen-Zhou, J.; Baldo, M. A.; Freedman, D. E.; Goldsmith, R. H.; Goodson, T.; Kirk, M. L.; McCusker, J. K.; Ogilvie, J. P.; Shultz, D. A.; Stoll, S.; Whaley, K. B. Exploiting Chemistry and Molecular Systems for Quantum Information Science. *Nat. Rev. Chem.* **2020**, *4*, 490–504.

(3) Bayliss, S. L.; Laorenza, D. W.; Mintun, P. J.; Kovos, B. D.; Freedman, D. E.; Awschalom, D. D. Optically Addressable Molecular Spins for Quantum Information Processing. *Science* **2020**, *370*, 1309–1312.

(4) Coronado, E. Molecular Magnetism: From Chemical Design to Spin Control in Molecules, Materials and Devices. *Nat. Rev. Mater.* **2020**, *5*, 87–104.

(5) Paquette, M. M.; Plaul, D.; Kurimoto, A.; Patrick, B. O.; Frank, N. L.; Patrick, B. O. Opto-Spintronics: Photoisomerization-Induced Spin State Switching at 300 K in Photochrome Cobalt-Dioxolene Thin Films. *J. Am. Chem. Soc.* **2018**, *140*, 14990–15000.

(6) Dei, A.; Gatteschi, D. Molecular (Nano) Magnets as Test Grounds of Quantum Mechanics. *Angew. Chem., Int. Ed.* **2011**, *50*, 11852–11858.

(7) Létard, J.-F.; Guionneau, P.; Goux-Capes, L. Towards Spin Crossover Applications. In *Spin Crossover Transition. Metal. Compounds,* Springer: Berlin, Heidelberg, 2004; Vol. 1, pp 221-249.

(8) Dei, A.; Gatteschi, D.; Sangregorio, C.; Sorace, L. Quinonoid Metal Complexes: Toward Molecular Switches. *Acc. Chem. Res.* **2004**, *37*, 827–835.

(9) Dugay, J.; Giménez-Marqués, M.; Kozlova, T.; Zandbergen, H. W.; Coronado, E.; Van Der Zant, H. S. J. Spin Switching in Electronic Devices Based on 2D Assemblies of Spin-Crossover Nanoparticles. *Adv. Mater.* **2015**, *27*, 1288–1293.

(10) Senthil Kumar, K.; Ruben, M. Emerging Trends in Spin Crossover (SCO) Based Functional Materials and Devices. *Coord. Chem. Rev.* **2017**, *346*, 176–205.

(11) Kahn, O.; Martinez, C. J. Spin-Transition Polymers: From Molecular Materials toward Memory Devices. *Science* **1998**, *279*, 44–48.

(12) Halcrow, M. a. The Foundation of Modern Spin-Crossover. *Chem. Commun.* **2013**, *49*, 10890.

(13) Tezgerevska, T.; Alley, K. G.; Boskovic, C. Valence Tautomerism in Metal Complexes: Stimulated and Reversible Intramolecular Electron Transfer between Metal Centers and Organic Ligands. *Coord. Chem. Rev.* **2014**, *268*, 23–40.

(14) Hendrickson, D. N.; Pierpont, C. G. Valence Tautomeric Transition Metal Complexes. In *Top Curr. Chem.,* Springer: Berlin, Heidelberg, 2004; Vol. 234, pp 63–95.

(15) Gransbury, G. K.; Boskovic, C. Valence Tautomerism in d-Block Complexes. *Encyclopedia of Inorganic and Bioinorganic Chemistry (online)*; John Wiley & Sons Ltd., 2021, in press.

(16) Wu, S.-Q.; Liu, M.; Gao, K.; Kanegawa, S.; Horie, Y.; Aoyama, G.; Okajima, H.; Sakamoto, A.; Baker, M. L.; Huzan, M. S.; Bencok, P.; Abe, T.; Shiota, Y.; Yoshizawa, K.;

Xu, W.; Kou, H.-Z.; Sato, O. Macroscopic Polarization Change via Electron Transfer in a Valence Tautomeric Cobalt Complex. *Nat. Commun.* **2020**, *11*, 1992.

(17) Nadurata, V. L.; Boskovic, C. Switching Metal Complexes via Intramolecular Electron Transfer: Connections with Solvatochromism. *Inorg. Chem. Front.* **2021**, *8*, 1840–1864.

(18) Wang, M.; Li, Z. Y.; Ishikawa, R.; Yamashita, M. Spin Crossover and Valence Tautomerism Conductors. *Coord. Chem. Rev.* **2021**, *435*, 213819.

(19) Calzolari, A.; Chen, Y.; Lewis, G. F.; Dougherty, D. B.; Shultz, D.; Buongiorno Nardelli, M. Complex Materials for Molecular Spintronics Applications: Cobalt Bis(Dioxolene) Valence Tautomers, from Molecules to Polymers. *J. Phys. Chem. B* **2012**, *116*, 13141–13148.

(20) Kanegawa, S.; Shiota, Y.; Kang, S.; Takahashi, K.; Okajima, H.; Sakamoto, A.; Iwata, T.; Kandori, H.; Yoshizawa, K.; Sato, O. Directional Electron Transfer in Crystals of [CrCo] Dinuclear Complexes Achieved by Chirality-Assisted Preparative Method. *J. Am. Chem. Soc.* **2016**, *138*, 14170–14173.

(21) Buchanan, R. M.; Pierpont, C. G. Tautomeric Catecholate-Semiquinone Interconversion via Metal-Ligand Electron Transfer. Structural, Spectral, and Magnetic Properties of (3,5-Di-Tert-Butylcatecholato)(3,5-Di-Tert-Butylsemiquinone)(Bipyridyl)Cobalt(III), a Complex Containing Mixed-Valence Organic Ligands. *J. Am. Chem. Soc.* **1980**, *102*, 4951–4957.

(22) Jung, O.-S.; Pierpont, C. G. Bistability and Low-Energy Electron Transfer in Cobalt Complexes Containing Catecholate and Semiquinone Ligands. *Inorg. Chem.* **1994**, *33*, 2227–2235.

(23) Adams, D. M.; Dei, A.; Rheingold, A. L.; Hendrickson, D. N.; Rheingold, A. L.; Dei, A. Bistability in the [Co^{II}(Semiquinonate)$_2$] to [Co^{III}(Catecholate)(Semiquinonate)] Valence-Tautomeric Conversion. *J. Am. Chem. Soc.* **1993**, *115*, 8221–8229.

(24) Adams, D. M.; Dei, A.; Rheingold, A. L.; Hendrickson, D. N. Controlling Valence Tautomerism of Cobalt Complexes Containing the Benzosemiquinone Anion as Ligand. *Angew. Chem., Int. Ed.* **1993**, *32*, 880–882.

(25) Hohenberg, P.; Kohn, W. Inhomogeneous Electron Gas. *Phys. Rev.* **1964**, *136*, B864–B871.

(26) Kohn, W.; Sham, L. J. Self-Consistent Equations Including Exchange and Correlation Effects. *Phys. Rev.* **1965**, *140*, A1133–A1138.

(27) Adams, D. M.; Noodleman, L.; Hendrickson, D. N. Density Functional Study of the Valence-Tautomeric Interconversion Low-Spin [Co^{III}(SQ)(Cat)(Phen)] ⇌ High-Spin [Co^{II}(SQ)$_2$(Phen)]. *Inorg. Chem.* **1997**, *36*, 3966–3984.

(28) Sato, D.; Shiota, Y.; Juhász, G.; Yoshizawa, K.; Juha, G.; Yoshizawa, K. Theoretical Study of the Mechanism of Valence Tautomerism in Cobalt Complexes. *J. Phys. Chem. Phys. Chem. A* **2010**, *114*, 12928–12935.

(29) Ivakhnenko, E. P.; Starikov, A. G.; Minkin, V. I.; Lyssenko, K. A.; Antipin, M. Y.; Simakov, V. I.; Korobov, M. S.; Borodkin, G. S.; Knyazev, P. A. Synthesis, Molecular and Electronic Structures of Six-Coordinate Transition Metal (Mn, Fe, Co, Ni, Cu, and Zn) Complexes with Redox-Active 9-Hydroxyphenoxazin-1-One Ligands. *Inorg. Chem.* **2011**, *50*, 7022–7032.

(30) Panja, A.; Jana, N. C.; Bauzá, A.; Frontera, A.; Mathonière, C. Solvent-Triggered Cis/Trans Isomerism in Cobalt Dioxolene Chemistry: Distinguishing Effects of Packing on Valence Tautomerism. *Inorg. Chem.* **2016**, *55*, 8331–8340.

(31) Bencini, A.; Caneschi, A.; Carbonera, C.; Dei, A.; Gatteschi, D.; Righini, R.; Sangregorio, C.; Slageren, J. Van. Tuning the Physical Properties of a Metal Complex by Molecular Techniques: The Design and the Synthesis of the Simplest Cobalt-o-Dioxolene Complex Undergoing Valence Tautomerism. *J. Mol. Struct.* **2003**, *656*, 141–154.

(32) Mörtel, M.; Seller, M.; Heinemann, F. W.; Khusniyarov, M. M. A Valence Tautomeric Cobalt–Dioxolene Complex with an Anchoring Group for Prospective Chemical Grafting to Metal Oxides. *Dalton Trans.* **2020**, *49*, 17532–17536.

(33) Tezgerevska, T.; Rousset, E.; Gable, R. W.; Jameson, G. N. L.; Sañudo, E. C.; Starikova, A.; Boskovic, C. Valence Tautomerism and Spin Crossover in Pyridinophane–Cobalt–Dioxolene Complexes: An Experimental and Computational Study. *Dalton Trans.* **2019**, *48*, 11674–11689.

(34) Gransbury, G. K.; Livesay, B. N.; Janetzki, J. T.; Hay, M. A.; Gable, R. W.; Shores, M. P.; Starikova, A.; Boskovic, C. Understanding the Origin of One- or Two-Step Valence Tautomeric Transitions in Bis(Dioxolene)-Bridged Dinuclear Cobalt Complexes. *J. Am. Chem. Soc.* **2020**, *142*, 10692–10704.

(35) Witt, A.; Heinemann, F. W.; Sproules, S.; Khusniyarov, M. M. Modulation of Magnetic Properties at Room Temperature: Coordination-Induced Valence Tautomerism in a Cobalt Dioxolene Complex. *Chem. - Eur. J.* **2014**, *20*, 11149–11162.

(36) Neese, F. Prediction of Molecular Properties and Molecular Spectroscopy with Density Functional Theory: From Fundamental Theory to Exchange-Coupling. *Coord. Chem. Rev.* **2009**, *253*, 526–563.

(37) Minkin, V. I.; Starikov, A. G.; Starikova, A. A. Computational Insight into Magnetic Behavior and Properties of the Transition Metal Complexes with Redox-Active Ligands: A DFT Approach. *Pure Appl. Chem.* **2018**, *90*, 811–824.

(38) Gransbury, G. K.; Boulon, M.-E.; Mole, R. A.; Gable, R. W.; Moubaraki, B.; Murray, K. S.; Sorace, L.; Soncini, A.; Boskovic, C. Single-Ion Anisotropy and Exchange Coupling in Cobalt(II)-Radical Complexes: Insights from Magnetic and Ab Initio Studies. *Chem. Sci.* **2019**, *10*, 8855–8871.

(39) Gransbury, G. K.; Boulon, M. E.; Petrie, S.; Gable, R. W.; Mulder, R. J.; Sorace, L.; Stranger, R.; Boskovic, C. DFT Prediction and Experimental Investigation of Valence Tautomerism in Cobalt-Dioxolene Complexes. *Inorg. Chem.* **2019**, *58*, 4230–4243.

(40) Chegerev, M. G.; Starikova, A. A.; Piskunov, A. V.; Cherkasov, V. K. Valence Tautomerism in Main-Group Complexes? Computational Modeling of Si, Ge, Sn, and Pb Bischelates with o-Iminoquinone Ligands. *Eur. J. Inorg. Chem.* **2016**, *2016*, 252–258.

(41) Chegerev, M. G.; Piskunov, A. V.; Starikova, A. A.; Kubrin, S. P.; Fukin, G. K.; Cherkasov, V. K.; Abakumov, G. A. Redox Isomerism in Main-Group Chemistry: Tin Complex with o-Iminoquinone Ligands. *Eur. J. Inorg. Chem.* **2018**, *2018*, 1087–1092.

(42) Phan, H.; Hrudka, J. J.; Igimbayeva, D.; Lawson Daku, L. M.; Shatruk, M. A Simple Approach for Predicting the Spin State of Homoleptic Fe(II) Tris-Diimine Complexes. *J.*

Am. Chem. Soc. **2017**, *139*, 6437–6447.

(43) McPherson, J. N.; Elton, T. E.; Colbran, S. B. A Strain-Deformation Nexus within Pincer Ligands: Application to the Spin States of Iron(II) Complexes. *Inorg. Chem.* **2018**, *57*, 12312–12322.

(44) Kershaw Cook, L. J.; Kulmaczewski, R.; Mohammed, R.; Dudley, S.; Barrett, S. A.; Little, M. A.; Deeth, R. J.; Halcrow, M. A. A Unified Treatment of the Relationship between Ligand Substituents and Spin State in a Family of Iron(II) Complexes. *Angew. Chem., Int. Ed.* **2016**, *55*, 4327–4331.

(45) Kimura, A.; Ishida, T. Spin-Crossover Temperature Predictable from DFT Calculation for Iron(II) Complexes with 4-Substituted Pybox and Related Heteroaromatic Ligands. *ACS Omega* **2018**, *3*, 6737–6747.

(46) Cirera, J.; Paesani, F. Theoretical Prediction of Spin-Crossover Temperatures in Ligand-Driven Light-Induced Spin Change Systems. *Inorg. Chem.* **2012**, *51*, 8194–8201.

(47) Zhang, Y. Predicting Critical Temperatures of Iron(II) Spin Crossover Materials: Density Functional Theory plus U Approach. *J. Chem. Phys.* **2014**, *141*, 214703.

(48) Martinho, P. N.; Martins, F. F.; Bandeira, N. A. G.; Calhorda, M. J. Spin Crossover in 3D Metal Centers Binding Halide-Containing Ligands: Magnetism, Structure and Computational Studies. *Sustainability* **2020**, *12*, 2512.

(49) Rodríguez-Jiménez, S.; Yang, M.; Stewart, I.; Garden, A. L.; Brooker, S. A Simple Method of Predicting Spin State in Solution. *J. Am. Chem. Soc.* **2017**, *139*, 18392–18396.

(50) Hearns, N. G. R.; Korčok, J. L.; Paquette, M. M.; Preuss, K. E. Dinuclear Cobalt Bis(Dioxolene) Complex Exhibiting Two Sequential Thermally Induced Valence Tautomeric Transitions. *Inorg. Chem.* **2006**, *45*, 8817–8819.

(51) Imaz, I.; Maspoch, D.; Rodríguez-Blanco, C.; Pérez-Falcón, J. M.; Campo, J.; Ruiz-Molina, D. Valence-Tautomeric Metal–Organic Nanoparticles. *Angew. Chem., Int. Ed.* **2008**, *120*, 1883–1886.

(52) O'Sullivan, T. J.; Djukic, B.; Dube, P. A.; Lemaire, M. T. A Conducting Metallopolymer Featuring Valence Tautomerism. *Chem. Commun.* **2009**, 1903–1905.

(53) Paquette, M. M.; Kopelman, R. A.; Beitler, E.; Frank, N. L. Incorporating Optical Bistability into a Magnetically Bistable System: A Photochromic Redox Isomeric Complex. *Chem. Commun.* **2009**, 5424–5426.

(54) Shultz, D. A.; Kumar, R. K.; Bin-Salamon, S.; Kirk, M. L. Valence Tautomerization and Exchange Coupling in a Cobalt- Nitronylnitroxide-Semiquinone Complex. *Polyhedron* **2005**, *24*, 2876–2879.

(55) Bin-Salamon, S.; Brewer, S.; Franzen, S.; Feldheim, D. L.; Lappi, S.; Shultz, D. A. Supramolecular Control of Valence-Tautomeric Equilibrium on Nanometer-Scale Gold Clusters. *J. Am. Chem. Soc.* **2005**, *127*, 5328–5329.

(56) Yoshida, Y.; Tanaka, H.; Saito, G.; Ouahab, L.; Yoshida, H.; Sato, N. Valence-Tautomeric Ionic Liquid Composed of a Cobalt Bis(Dioxolene) Complex Dianion. *Inorg. Chem.* **2009**, *48* , 9989–9991.

(57) Kiriya, D.; Chang, H. C.; Kamata, A.; Kitagawa, S. Polytypic Phase Transition in Alkyl Chain-Functionalized Valence Tautomeric Complexes. *J. Chem. Soc. Dalton Trans.* **2006**, *60*, 1377–1382.

(58) Mulyana, Y.; Poneti, G.; Moubaraki, B.; Murray, K. S.; Abrahams, B. F.; Sorace, L.; Boskovic, C. Solvation Effects on the Valence Tautomeric Transition of a Cobalt Complex in the Solid State. *Dalton Trans.* **2010**, *39*, 4757–4767.

(59) Antipin, M. Y.; Ivakhnenko, E. P.; Koshchienko, Y. V.; Knyazev, P. A.; Korobov, M. S.; Chernyshev, A. V.; Lyssenko, K. A.; Starikov, A. G.; Minkin, V. I. Adducts of Cobalt(II) Bis(Salicylaldiminates) and Redox-Active Phenoxazin-1-One: Synthesis, Structure, and Magnetic Properties. *Russ. Chem. Bull.* **2013**, *62*, 1744–1751.

(60) Llunell, M.; Casanova, D.; Cirera, J.; Alemany, P.; Alvarez, S. *SHAPE, 2.1*; Universitat de Barcelona: Barecelona, Spain 2013.

(61) Alvarez, S.; Avnir, D.; Llunell, M.; Pinsky, M. Continuous Symmetry Maps and Shape Classification. The Case of Six-Coordinated Metal Compounds. *New J. Chem.* **2002**, *26*, 996–1009.

(62) Ketkaew, R.; Tantirungrotechai, Y.; Harding, P.; Chastanet, G.; Guionneau, P.; Marchivie, M.; Harding, D. J. OctaDist: A Tool for Calculating Distortion Parameters in Spin Crossover and Coordination Complexes. *Dalton Trans.* **2021**, *50*, 1086–1096.

(63) Aragão, D.; Aishima, J.; Cherukuvada, H.; Clarken, R.; Clift, M.; Cowieson, N. P.; Ericsson, D. J.; Gee, C. L.; Macedo, S.; Mudie, N.; Panjikar, S.; Price, J. R.; Riboldi-Tunnicliffe, A.; Rostan, R.; Williamson, R.; Caradoc-Davies, T. T. MX2: A High-Flux

Undulator Microfocus Beamline Serving Both the Chemical and Macromolecular Crystallography Communities at the Australian Synchrotron. *J. Synchrotron Radiat.* **2018**, *25*, 885–891.

(64) Lynch, M. W.; Valentine, M.; Hendrickson, D. N. Mixed-Valence Semiquinone-Catecholate-Iron Complexes. *J. Am. Chem. Soc.* **1982**, *104*, 6982–6989.

(65) Alley, K. G.; Poneti, G.; Robinson, P. S. D.; Nafady, A.; Moubaraki, B.; Aitken, J. B.; Drew, S. C.; Ritchie, C.; Abrahams, B. F.; Hocking, R. K.; Murray, K. S.; Bond, A. M.; Harris, H. H.; Sorace, L.; Boskovic, C. Redox Activity and Two-Step Valence Tautomerism in a Family of Dinuclear Cobalt Complexes with a Spiroconjugated Bis(Dioxolene) Ligand. *J. Am. Chem. Soc.* **2013**, *135*, 8304–8323.

(66) Adams, D. M.; Hendrickson, D. N. Pulsed Laser Photolysis and Thermodynamics Studies of Intramolecular Electron Transfer in Valence Tautomeric Cobalt o-Quinone Complexes. *J. Am. Chem. Soc.* **1996**, *118*, 11515–11528.

(67) Slichter, C. P.; Drickamer, H. G. Pressure-Induced Electronic Changes in Compounds of Iron. *J. Chem. Phys.* **1972**, *56*, 2142–2160.

(68) Hirata, S.; Head-Gordon, M. Time-Dependent Density Functional Theory within the Tamm–Dancoff Approximation. *Chem. Phys. Lett.* **1999**, *314*, 291–299.

(69) Neese, F. The ORCA Program System. *Wiley Interdiscip. Rev. Comput. Mol. Sci.* **2012**, *2*, 73–78.

(70) Neese, F. Software Update: The ORCA Program System, Version 4.0. *WIREs Comput. Mol.*

Sci. **2018**, *8*, 4–9.

(71) Becke, A. D. A New Mixing of Hartree-Fock and Local Density-Functional Theories. *J. Chem. Phys.* **1993**, *98*, 1372–1377.

(72) Stephens, P. J.; Devlin, F. J.; Chabalowski, C. F.; Frisch, M. J. Ab Initio Calculation of Vibrational Absorption and Circular Dichroism Spectra Using Density Functional Force Fields. *J. Phys. Chem.* **1994**, *98*, 11623–11627.

(73) De, S.; Chamoreau, L.-M.; El Said, H.; Li, Y.; Flambard, A.; Boillot, M.-L.; Tewary, S.; Rajaraman, G.; Lescouëzec, R. Thermally-Induced Spin Crossover and LIESST Effect in the Neutral $[Fe^{II}(Mebik)_2(NCX)_2]$ Complexes: Variable-Temperature Structural, Magnetic, and Optical Studies (X = S, Se; Mebik = Bis(1-Methylimidazol-2-Yl)Ketone). *Front. Chem.* **2018**, *6*, 1–15.

(74) McClintock, L. F.; Bagaria, P.; Kjaergaard, H. G.; Blackman, A. G. Co(III) Complexes of the Type $[(L)Co(O_2CO)]^+$ (L = Tripodal Tetraamine Ligand): Synthesis, Structure, DFT Calculations and ^{59}Co NMR. *Polyhedron* **2009**, *28*, 1459–1468.

(75) Tozer, D. J. Relationship between Long-Range Charge-Transfer Excitation Energy Error and Integer Discontinuity in Kohn–Sham Theory. *J. Chem. Phys.* **2003**, *119*, 12697–12699.

(76) Dreuw, A.; Head-Gordon, M. Failure of Time-Dependent Density Functional Theory for Long-Range Charge-Transfer Excited States: The Zincbacteriochlorin−Bacteriochlorin and Bacteriochlorophyll−Spheroidene Complexes. *J. Am. Chem. Soc.* **2004**, *126*, 4007–4016.

(77) Goerigk, L.; Casanova-Paéz, M. The Trip to the Density Functional Theory Zoo Continues:

Making a Case for Time-Dependent Double Hybrids for Excited-State Problems. *Aust. J. Chem.* **2021**, *74*, 3.

(78) Rosa, A.; Ricciardi, G.; Gritsenko, O.; Baerends, E. J. Excitation Energies of Metal Complexes with Time-Dependent Density Functional Theory. In *Principles and Applications of Density Functional Theory in Inorganic Chemistry I. Structure and Bonding*; Springer Berlin Heidelberg: Berlin, Heidelberg, 2004; pp 49–116.

(79) Casanova-Páez, M.; Goerigk, L. Assessing the Tamm–Dancoff Approximation, Singlet–Singlet, and Singlet–Triplet Excitations with the Latest Long-Range Corrected Double-Hybrid Density Functionals. *J. Chem. Phys.* **2020**, *153*, 064106.

(80) Yanai, T.; Tew, D. P.; Handy, N. C. A New Hybrid Exchange-Correlation Functional Using the Coulomb-Attenuating Method (CAM-B3LYP). *Chem. Phys. Lett.* **2004**, *393*, 51–57.

(81) Chai, J.-D.; Head-Gordon, M. Systematic Optimization of Long-Range Corrected Hybrid Density Functionals. *J. Chem. Phys.* **2008**, *128*, 084106.

(82) Hickson, J. R.; Horsewill, S. J.; McGuire, J.; Wilson, C.; Sproules, S.; Farnaby, J. H. The Semiquinone Radical Anion of 1,10-Phenanthroline-5,6-Dione: Synthesis and Rare Earth Coordination Chemistry. *Chem. Commun.* **2018**, *54*, 11284–11287.

(83) Mera-Adasme, R.; Xu, W. H.; Sundholm, D.; Mendizabal, F. Calculations of the Light Absorption Spectra of Porphyrinoid Chromophores for Dye-Sensitized Solar Cells. *Phys. Chem. Chem. Phys.* **2016**, *18*, 27877–27884.

(84) Pierpont, C. G.; Jung, O.-S. S. Thermodynamic Parameters for Cobalt-Quinone Electron

Transfer and Spin Transition Steps of the Co^{III}(Bpy)(3,5-DBSQ)(3,5-DBCat)/Co^{II}(Bpy)(3,5-DBSQ)$_2$ Valence Tautomeric Equilibrium. *Inorg. Chem.* **1995**, *34*, 4281–4283.

(85) Patchkovskii, S.; Ziegler, T. Improving "Difficult" Reaction Barriers with Self-Interaction Corrected Density Functional Theory. *J. Chem. Phys.* **2002**, *116*, 7806–7813.

(86) Zhang, Y.; Yang, W. A Challenge for Density Functionals: Self-Interaction Error Increases for Systems with a Noninteger Number of Electrons. *J. Chem. Phys.* **1998**, *109*, 2604–2608.

(87) Bao, J. L.; Gagliardi, L.; Truhlar, D. G. Self-Interaction Error in Density Functional Theory: An Appraisal. *J. Phys. Chem. Lett.* **2018**, *9*, 2353–2358.

(88) Lonsdale, D. R.; Goerigk, L. The One-Electron Self-Interaction Error in 74 Density Functional Approximations: A Case Study on Hydrogenic Mono- And Dinuclear Systems. *Phys. Chem. Chem. Phys.* **2020**, *22*, 15805–15830.

(89) Dowling, C.; Dinsdale, D. R.; Lemaire, M. T. Preparation, Electrochemical Behavior, and Variable-Temperature Magnetic Properties of Co(3,5-DBSQ)$_2$ Complexes of Imidazole-or Pyrazole-Substituted Ligands. *Can. J. Chem.* **2015**, *93*, 769–774.

(90) Becke, A. D. Correlation Energy of an Inhomogeneous Electron Gas: A Coordinate-space Model. *J. Chem. Phys.* **1988**, *88*, 1053–1062.

(91) Perdew, J. P.; Burke, K.; Ernzerhof, M. Generalized Gradient Approximation Made Simple. *Phys. Rev. Lett.* **1996**, *77*, 3865–3868.

(92) Minenkov, Y.; Singstad, Å.; Occhipinti, G.; Jensen, V. R. The Accuracy of DFT-Optimized

Geometries of Functional Transition Metal Compounds: A Validation Study of Catalysts for Olefin Metathesis and Other Reactions in the Homogeneous Phase. *Dalton Trans.* **2012**, *41*, 5526–5541.

(93) Reiher, M.; Salomon, O.; Artur Hess, B. Reparameterization of Hybrid Functionals Based on Energy Differences of States of Different Multiplicity. *Theor. Chem. Acc.* **2001**, *107*, 48–55.

(94) Lee, C.; Yang, W.; Parr, R. G. Development of the Colle-Salvetti Correlation-Energy Formula into a Functional of the Electron Density. *Phys. Rev. B* **1988**, *37*, 785–789.

(95) Handy, N. C.; Cohen, A. J. Left-Right Correlation Energy. *Mol. Phys.* **2001**, *99*, 403–412.

(96) Grimme, S.; Brandenburg, J. G.; Bannwarth, C.; Hansen, A. Consistent Structures and Interactions by Density Functional Theory with Small Atomic Orbital Basis Sets. *J. Chem. Phys.* **2015**, *143*, 054107.

(97) Grimme, S.; Antony, J.; Ehrlich, S.; Krieg, H. A Consistent and Accurate Ab Initio Parametrization of Density Functional Dispersion Correction (DFT-D) for the 94 Elements H-Pu. *J. Chem. Phys.* **2010**, *132*, 154104.

(98) Grimme, S.; Ehrlich, S.; Goerigk, L. Effect of the Damping Function in Dispersion Corrected Density Functional Theory. *J. Comput. Chem.* **2011**, *32*, 1456–1465.

(99) Kruse, H.; Grimme, S. A Geometrical Correction for the Inter- and Intra-Molecular Basis Set Superposition Error in Hartree-Fock and Density Functional Theory Calculations for Large Systems. *J. Chem. Phys.* **2012**, *136*, 154101.

(100) Noodleman, L. Valence Bond Description of Antiferromagnetic Coupling in Transition Metal Dimers. *J. Chem. Phys.* **1981**, *74*, 5737–5743.

(101) Van Lenthe, E.; Baerends, E. J.; Snijders, J. G. Relativistic Total Energy Using Regular Approximations. *J. Chem. Phys.* **1994**, *101*, 9783–9792.

(102) Weigend, F.; Ahlrichs, R. Balanced Basis Sets of Split Valence, Triple Zeta Valence and Quadruple Zeta Valence Quality for H to Rn: Design and Assessment of Accuracy. *Phys. Chem. Chem. Phys.* **2005**, *7*, 3297–3305.

(103) Takano, Y.; Houk, K. N. Benchmarking the Conductor-like Polarizable Continuum Model (CPCM) for Aqueous Solvation Free Energies of Neutral and Ionic Organic Molecules. *J. Chem. Theory Comput.* **2005**, *1*, 70–77.

(104) Mardirossian, N.; Head-Gordon, M. Mapping the Genome of Meta-Generalized Gradient Approximation Density Functionals: The Search for B97M-V. *J. Chem. Phys.* **2015**, *142*, 074111.

(105) Najibi, A.; Goerigk, L. DFT-D4 Counterparts of Leading Meta-Generalized-Gradient Approximation and Hybrid Density Functionals for Energetics and Geometries. *J. Comput. Chem.* **2020**, *41*, 2562–2572.

(106) Najibi, A.; Goerigk, L. The Nonlocal Kernel in van Der Waals Density Functionals as an Additive Correction: An Extensive Analysis with Special Emphasis on the B97M-V and ωB97M-V Approaches. *J. Chem. Theory Comput.* **2018**, *14*, 5725–5738.

(107) Zhao, Y.; Truhlar, D. G. A New Local Density Functional for Main-Group

Thermochemistry, Transition Metal Bonding, Thermochemical Kinetics, and Noncovalent Interactions. *J. Chem. Phys.* **2006**, *125*, 194101.

(108) Staroverov, V. N.; Scuseria, G. E.; Tao, J.; Perdew, J. P. Comparative Assessment of a New Nonempirical Density Functional: Molecules and Hydrogen-Bonded Complexes. *J. Chem. Phys.* **2003**, *119*, 12129–12137.

(109) Mardirossian, N.; Head-Gordon, M. ΩB97X-V: A 10-Parameter, Range-Separated Hybrid, Generalized Gradient Approximation Density Functional with Nonlocal Correlation, Designed by a Survival-of-the-Fittest Strategy. *Phys. Chem. Chem. Phys.* **2014**, *16*, 9904–9924.

(110) Grimme, S. Semiempirical Hybrid Density Functional with Perturbative Second-Order Correlation. *J. Chem. Phys.* **2006**, *124*, 034108.

(111) Radoń, M. Benchmarking Quantum Chemistry Methods for Spin-State Energetics of Iron Complexes against Quantitative Experimental Data. *Phys. Chem. Chem. Phys.* **2019**, *21*, 4854–4870.

(112) Goerigk, L.; Grimme, S. A Thorough Benchmark of Density Functional Methods for General Main Group Thermochemistry, Kinetics, and Noncovalent Interactions. *Phys. Chem. Chem. Phys.* **2011**, *13*, 6670–6688.

(113) Caldeweyher, E.; Ehlert, S.; Hansen, A.; Neugebauer, H.; Spicher, S.; Bannwarth, C.; Grimme, S. A Generally Applicable Atomic-Charge Dependent London Dispersion Correction. *J. Chem. Phys.* **2019**, *150*, 154122.

(114) Caldeweyher, E.; Bannwarth, C.; Grimme, S. Extension of the D3 Dispersion Coefficient Model. *J. Chem. Phys.* **2017**, *147*, 034112.

(115) Hammett, L. P. The Effect of Structure upon the Reactions of Organic Compounds. Temperature and Solvent Influences. *J. Chem. Phys.* **1936**, *4*, 613–617.

(116) Genix, P.; Jullien, H.; Le Goas, R. Estimation of Hammett Sigma Constants from Calculated Atomic Charges Using Partial Least Squares Regression. *J. Chemom.* **1996**, *10*, 631–636.

(117) Paquette, M. M.; Patrick, B. O.; Frank, N. L. Determining the Magnitude and Direction of Photoinduced Ligand Field Switching in Photochromic Metal - Organic Complexes: Molybdenum - Tetracarbonyl Spirooxazine Complexes. *J. Am. Chem. Soc.* **2011**, *133*, 10081–10093.

(118) Farrell, I. R.; Hartl, F.; Záliš, S.; Mahabiersing, T.; Vlček, Jr, A. The Spectroscopic, Electrochemical and Photophysical Effects of the B1/A2 Π* Lowest Unoccupied Molecular Orbital Switching in $[M(CO)_4(N,N)]$ (M = Cr or W; N,N = 1,10-Phenanthroline or 3,4,7,8-Tetramethyl-1,10-Phenanthroline). An Experimental and DFT Comput. *J. Chem. Soc. Dalton Trans.* **2000**, 4323–4331.

(119) Ernst, S.; Vogler, C.; Klein, A.; Kaim, W.; Zališ, S. Π* Molecular Orbital Crossing A2(χ)/B1(ψ) in 1,10-Phenanthroline Derivatives. Ab Initio Calculations and EPR/ENDOR Studies of the 4,7-Diaza-1,10-Phenanthroline Radical Anion and Its $M(CO)_4$ Complexes (M = Cr, Mo, W). *Inorg. Chem.* **1996**, *35*, 1295–1300.

(120) Nakano, K.; Suemura, N.; Yoneda, K.; Kawata, S.; Kaizaki, S. Substituent Effect of the Coordinated Pyridine in a Series of Pyrazolato Bridged Dinuclear Diiron(II) Complexes on

the Spin-Crossover Behavior. *Dalton Trans.* **2005**, *2*, 740.

(121) Prat, I.; Company, A.; Corona, T.; Parella, T.; Ribas, X.; Costas, M. Assessing the Impact of Electronic and Steric Tuning of the Ligand in the Spin State and Catalytic Oxidation Ability of the Fe^{II}(Pytacn) Family of Complexes. *Inorg. Chem.* **2013**, *52*, 9229–9244.

(122) Houghton, B. J.; Deeth, R. J. Spin-State Energetics of Feii Complexes - The Continuing Voyage through the Density Functional Minefield. *Eur. J. Inorg. Chem.* **2014**, *2014* , 4573–4580.

(123) Takahashi, K.; Hasegawa, Y.; Sakamoto, R.; Nishikawa, M.; Kume, S.; Nishibori, E.; Nishihara, H. Solid-State Ligand-Driven Light-Induced Spin Change at Ambient Temperatures in Bis(Dipyrazolylstyrylpyridine)Iron(II) Complexes. *Inorg. Chem.* **2012**, *51*, 5188–5198.

(124) Park, J. G.; Jeon, I.-R.; Harris, T. D. Electronic Effects of Ligand Substitution on Spin Crossover in a Series of Diiminoquinonoid-Bridged Fe^{II}_2 Complexes. *Inorg. Chem.* **2015**, *54*, 359–369.

(125) Lin, H. J.; Siretanu, D.; Dickie, D. A.; Subedi, D.; Scepaniak, J. J.; Mitcov, D.; Clérac, R.; Smith, J. M. Steric and Electronic Control of the Spin State in Three-Fold Symmetric, Four-Coordinate Iron(II) Complexes. *J. Am. Chem. Soc.* **2014**, *136*, 13326–13332.

(126) Phonsri, W.; Harding, D. J.; Harding, P.; Murray, K. S.; Moubaraki, B.; Gass, I. A.; Cashion, J. D.; Jameson, G. N. L.; Adams, H. Stepped Spin Crossover in Fe(III) Halogen Substituted Quinolylsalicylaldimine Complexes. *Dalton Trans.* **2014**, *43*, 17509–17518.

SYNOPSIS

A density functional theory strategy has been developed to provide accurate and simple prediction of transition temperatures for [Co(dbdiox)(dbsq)(N_2L)] valence tautomeric complexes.